SIAM J. NUMER. ANAL.
Vol. 56, No. 6, pp. 3358–3385

A NEW NUMERICAL APPROACH TO INVERSE TRANSPORT EQUATION WITH ERROR ANALYSIS*

QIN LI†, RUIWEN SHU‡, AND LI WANG§

Abstract. The inverse radiative transfer problem finds broad applications in medical imaging, atmospheric science, astronomy, and many other areas. This problem intends to recover optical properties, denoted as absorption and the scattering coefficient of the media, through source-measurement pairs. A typical computational approach is to form the inverse problem as a PDE-constraint optimization, with the minimizer being the to-be-recovered coefficients. The method is tested to be efficient in practice, but it lacks analytical justification: there is no guarantee of the existence or uniqueness of the minimizer, and the error is hard to quantify. In this paper, we provide a different algorithm by levering the ideas from singular decomposition analysis. Our approach is to decompose the measurements into three components, two of which encode the information of the two coefficients, respectively. We then split the optimization problem into two subproblems and use those two components to recover the absorption and scattering coefficients *separately*. In this regard, we prove the well-posedness of the new optimization, and the error could be quantified with better precision. In the end, we incorporate the diffusive scaling and show that the error is harder to control in the diffusive limit.

Key words. inverse problem, radiative transfer, optimization, singular decomposition

AMS subject classifications. 65N20, 65N21, 65R20, 65R32

DOI. 10.1137/17M1142697

1. Introduction.

The radiative transfer equation (RTE) describes the dynamics of (photon) particles in materials with various optical properties. It has been used as a basic model in atmospheric science, medical imaging, and many other areas. The equation can take different forms, depending on the degrees of generality. Among them, a stationary, frequency independent form reads

$$v \cdot \nabla_x f + \sigma(x) f = \int k(x, v, v') f(x, v') \mathrm{d}v' \,, \tag{1}$$

where $f(x, v)$, defined on phase space, is the distribution of particles at location x and with velocity v. Here $x \in \Omega \subset \mathbb{R}^d$ with $d = 2, 3$, and $v \in V = \mathbb{S}^{d-1}$, the *unit* sphere in $\mathbb{R}^d$. $k(x, v, v')$ is termed the scattering coefficient, representing the probability of particles moving in direction v' changing to direction v at location x. $\sigma(x)$ is the total absorption coefficient that represents a certain amount of photon particles being absorbed by the material. Here we assume that σ has no velocity dependence. The

*Received by the editors August 8, 2017; accepted for publication (in revised form) October 1, 2018; published electronically November 29, 2018.
http://www.siam.org/journals/sinum/56-6/M114269.html

Funding: The work of the first author was supported in part by National Science Foundation grants DMS-1619778, DMS-1750488, and DMS-1107291: RNMS KI-Net. The work of the second author was supported in part by National Science Foundation grants DMS-1522184 and DMS-1107291: RNMS KI-Net. The work of the third author was supported in part by a start-up fund from SUNY Buffalo and University of Minnesota, and by National Science Foundation grant DMS-1620135 1903420.

†Mathematics Department and Wisconsin Institutes for Discovery, University of Wisconsin-Madison, Madison, WI 53705 (qinli@math.wisc.edu).

‡Department of Mathematics, University of Maryland, College Park, College Park, MD 20742 (rshu@cscamm.umd.edu).

§School of Mathematics, University of Minnesota, Minneapolis, MN 55455 (wang8818@umn.edu).

boundary is separated into an "outgoing" and an "incoming" part by defining

$$\Gamma_{\pm} = \{(x,v) : x \in \partial\Omega\,, \pm v \cdot n_x > 0\}\,, \tag{2}$$

where n_x is the normal direction pointing out of Ω at $x \in \partial\Omega$. In this way, Γ_- collects all boundary coordinates that represent particles coming into the domain where Γ_+ collects the opposite. For the well-posedness of RTE, we require an inflow boundary condition, i.e., the data imposed on the "incoming" part of Γ_-:

$$f|_{\Gamma_-} = f_-(x,v)\,, \quad (x,v) \in \Gamma_-\,. \tag{3}$$

In many applications, light is sent to a bulk of material with unknown absorption and scattering properties, and light current propagating out of the material is measured. Scientists need to adjust the sources and measurement locations for recovering the material properties. This technique is used in medical imaging, where near infrared light (NIR) is sent into biological tissue to determine tumor or bone structure [26, 27]. It is also used in astronomical studies: during its travel around Jupiter, the unmanned spacecraft Galileo captured images using a near infrared mapping spectrometer (NIMS), and scientists recovered atmospheric components of Jupiter's moons by inverting RTE, through which they found that Io is covered mainly by SO_2 [16].

We study these problems from both a mathematical and computational point of view. Mathematically, we typically assume that no prior information on σ and k is known but that the entire incoming-to-outgoing map is given. This map is termed the *albedo* operator:

$$\mathcal{A}l : \qquad f_- \mapsto f\big|_{\Gamma_+}\,. \tag{4}$$

Then the goal of inverse RTE is to recover σ and k through the albedo operator.

The well-posedness of this problem was considered in [15], in which the authors showed that, given the albedo operator (4), a full recovery of both σ and k is possible in 3D, whereas in 2D only σ is recoverable. Some follow-up studies included utilizing the Born series for the recovery [24]; the ill-posedness of the problem if the operator's output was changed to flow current (having no velocity angle information) [7, 6]; the passage to the ill-posedness in the fluid regime [13]; and studies on various scenarios [8, 5]. Most of these analytical studies use the technique termed "singular decomposition" introduced in [15]. In that paper, the authors separate the data according to the singularities of different components in the measurement, each of which is in charge of recovering one property. See also the review in [4]. However, despite its effectiveness in analysis, singular decomposition is rarely used directly in computation because it is not known whether the process could be repeated numerically or in a real experiment, and because of the error analysis it lacks in practice.

From the computational viewpoint, the topic has been extensively studied in many scenarios [33, 21, 30, 14, 1]. Reviews can be found in [2, 3, 29]. One typical formulation is to first rewrite the equation in an optimization form and then run optimization algorithms for the recovery. More specifically, one samples N_x and N_v grids for x and v, respectively, and writes the equation in the following discrete form:

$$(\mathsf{A} + \mathsf{B}) \cdot \mathbf{f} = \mathbf{0} \quad \text{with} \quad \mathbf{f}|_{\Gamma_-} = \mathbf{f}_-\,.$$

Here $\mathbf{f}$ is the solution sampled on all grid points,

$$\mathbf{f} = [f(x_1,v_1), f(x_2,v_1), \ldots, f(x_n,v_1), f(x_1,v_2), \ldots, f(x_{N_x},v_2), \ldots, \ldots, f(x_{N_x},v_{N_v})]^t, \tag{5}$$

and $\mathbf{f}_-$ is f_- evaluated on grid points on Γ_-. Considering the dimension of x and v, the subscript i and j can be multi-indexed. The equation

$$-\mathsf{A} = \mathsf{V} \otimes \nabla_x + \mathsf{I} \otimes \sigma, \quad \mathsf{B} = \Sigma_k\,, \tag{6}$$

shows the discrete version of the transport and the scattering operator, where V is a diagonal matrix of size $N_v \times N_v$ with diagonal elements v_i, and ∇_x is an $N_x \times N_x$ finite difference matrix in x (depending on the scheme one uses). σ is an $N_x \times N_x$ matrix with diagonals $\sigma(x_i)$, and Σ_k is a block matrix with N_x blocks, where each block is of size $N_v \times N_v$.

Given several rounds of experiments with $\{\mathbf{f}_-^{(i)}\,, i = 1, \ldots, N_I\}$ as the inflow on Γ_-, and the measured data $\{\phi^{(i)}\,, i = 1, \ldots, N_I\}$ as the outflow on Γ_+, the typical setup of the numerical inverse problem is to perform the following optimization problem:

$$\begin{cases} \min_{\sigma, \Sigma_k, \{\mathbf{f}^{(i)}\}} \sum_i \|\mathsf{E}_+ \mathbf{f}^{(i)} - \phi^{(i)}\| + \text{regularization} \\ \quad \text{s.t.} \quad (\mathsf{A} + \mathsf{B}) \cdot \mathbf{f}^{(i)} = \mathbf{0}\,, \quad \mathsf{E}_- \mathbf{f}^{(i)} = \mathbf{f}_-^{(i)} \quad \forall i. \end{cases} \tag{7}$$

Here the superscript i denotes different experiments, and E is the confining operator,

$$\mathsf{E}_\pm \mathbf{f} = \mathbf{f}|_{\Gamma_\pm}\,. \tag{8}$$

One advantage of this approach is that it is very straightforward, and the regularization could be adjusted to fit a priori information (for example, a TV norm used on σ for piecewise constant cases). The disadvantage is obvious as well, as mentioned in [29]: on one hand, it is not known whether the minimizer exists, or is unique, and the problem tends to be either overdetermined or underdetermined; on the other hand, the computational size is huge. There are N_x unknowns in σ and $N_x N_v$ unknowns in Σ_k, and in the $d = 3$ case, N_x is approximately N^3 and N_v is approximately N^2, with N being the number of grid points per direction. It is extremely expensive to update even one iteration in the optimization problem. Multiple strategies are invented as modifications for better efficiency, such as utilizing the diffusion approximation [32, 34], employing linearization [29], or computing the gradient on-the-fly for the updating [31] instead of preparing the Jacobian function ahead of time. However, despite all efforts the well-posedness results from the analysis do not benefit the computation, and it is extremely hard to quantify the error of any of these methods.

In this paper, we intend to bridge the gap between analysis and computation. More specifically, we will design an algorithm that (a) is efficient, and (b) leverages as much of the analysis results as possible. This allows us to spell out the well-posedness and the error analysis in an exact fashion numerically. Our idea is based on singular decomposition analysis, and we will numerically separate the three components in the measurements, using one to recover σ and another for k.

More precisely, consider concentrated incoming data f_-, and let $\phi(x, v)$ be the solution of (1) confined on Γ_+: $\phi = f\big|_{\Gamma_+}$; then the analysis in [15] tells us that $\phi = \phi_1 + \phi_2 + \phi_3$ with its components enjoying different singularities and thus able to be separated from one other. Specifically, with ϕ_1 separated from the rest, it could be used to recover σ,

$$\mathcal{R}[\sigma] = \int_0^{\tau_-(x,v)} \sigma(x - sv) ds = \ln\left(\frac{f_-(x - \tau_-(x,v)v, v)}{\phi_1(x,v)}\right),$$

where τ_- is the time needed for a nonscattering photon passing through Ω and emitting at $(x,v) \in \Gamma_+$. $\mathcal{R}$ is the X-ray transform that has been proved to be reversible. We repeat this procedure numerically. Denote by $\phi_{R,1}$ the first component that gets extracted numerically from ϕ; we show that (see Theorem 3)

$$\frac{|\phi_{R,1} - \phi_1|}{|\phi_1|} = \mathcal{O}(\varepsilon_1^{1-\delta}\varepsilon) \quad \text{for any } \delta > 0\,, \tag{9}$$

with ε_1 and ε standing for the width of the concentrating inflow data and outflow measurement, respectively. Consequently, the numerically recovered σ has the following error estimate (see Theorem 4):

$$\|\Sigma - \sigma^{dis}\|_2 \lesssim (\varepsilon_1^{1-\delta}\varepsilon + \Delta x^2)^{1/2}\,,$$

where σ^{dis} is the true absorption coefficient evaluated at the grid points, and Δx is the discretization in x. Here we only analyze the recovery of σ. We believe that similar analysis can be done, for the scattering coefficient k, but it will be much more involved, and so we leave it for future work. At the end of this paper, we also study the inverse RTE in the diffusion regime using this approach. When the RTE can be well approximated by the diffusion equation, one gains a large error in the data separation step (9), and this error propagates in recovering σ. The whole scheme therefore breaks down. This analysis indicates that our approach works only for the weak scattering case.

The rest of the paper is organized as follows. In the next section, we recall the singular decomposition theory used in proving the well-posedness of the inverse problem, and we make an analogy in the discrete setting. In section 3, we set up the new algorithm and provide details in the implementation. Section 4 is devoted to the error analysis, which consists of two major parts: error in the data separation and inversion. In section 5, we introduce a diffusive scaling to the RTE and revisit the algorithms and error analysis in the presence of multiple scales.

2. Singular decomposition. The basis of our algorithm is the singular decomposition to the measured data. In this section, we first review this technique, developed in [15], and then extend it in the discrete setting that we will be working on. Let us denote

$$\mathcal{A} = -v \cdot \nabla_x - \sigma(x), \quad \mathcal{B}f = \int k(x,v,v')f(v')dv'\,; \tag{10}$$

then equation (1) can be rewritten as $(\mathcal{A}+\mathcal{B})f = 0$. One sees that $\mathcal{A}$ consists of a free transport and damping, whereas $\mathcal{B}$ encodes the scattering. We let

$$\tau_\pm(x,v) = \min\{t \geq 0,\ x \pm tv \in \partial\Omega\}$$

be the time for a free transport of a photon located at x with velocity v to travel out of Ω forward or backward, and we denote $\tau = \tau_- + \tau_+$. We also assume that

$$\sigma(x) - \int k(x,v,v')dv' \geq \nu > 0, \quad \text{for a.e. } (x,v) \in \Omega \times V\,,$$

in which case the forward problem (1) is well-posed, and the (σ, k) pair is called admissible.

2.1. Continuous setting. Singular decomposition is proposed in [15] for the continuous setting. The idea is that when the incoming data are concentrated around one point in $\Omega \times \Gamma_-$ space, the solution to (1) can be decomposed into three parts that enjoy different degrees of singularity, wherein the leading two singular terms can be used to recover σ and k, respectively. Indeed, formally one can write the solution to

$$\begin{cases} (\mathcal{A}+\mathcal{B})f = 0, & (x,v) \in \Omega \times V, \\ f\big|_{\Gamma_-} = f_-(x,v) \end{cases} \tag{11}$$

as

$$\begin{aligned} f &= (I + \mathcal{A}^{-1}\mathcal{B})^{-1}\mathcal{J}f_- \\ &= \mathcal{J}f_- - (\mathcal{A}^{-1}\mathcal{B})\mathcal{J}f_- + (I+\mathcal{A}^{-1}\mathcal{B})^{-1}(\mathcal{A}^{-1}\mathcal{B})^2\mathcal{J}f_- \\ &:= f_1 + f_2 + f_3\,, \end{aligned} \tag{12}$$

where $\mathcal{J} : \Gamma_- \to \Omega \times V$ is the solution to the pure transport and damping, i.e.,

$$\mathcal{A}(\mathcal{J}f_-) = 0, \quad \mathcal{J}f_-\big|_{\Gamma_-} = f_-\,. \tag{13}$$

It maps the boundary condition to the entire $\Omega \times V$, with an explicit form

$$\mathcal{J}f_-(x,v) = e^{-\int_0^{\tau_-(x,v)} \sigma(x-sv)\mathrm{d}s} f_-(x-\tau_-(x,v)v, v)\,. \tag{14}$$

The inverse of $\mathcal{A}$, denoted as $\mathcal{A}^{-1} : \Omega \times V \to \Omega \times V$, has the form

$$\mathcal{A}^{-1}f = -\int_0^{\tau_-(x,v)} e^{-\int_0^t \sigma(x-sv)\mathrm{d}s} f(x-tv, v)\mathrm{d}t\,.$$

It satisfies $\mathcal{A}(\mathcal{A}^{-1}f) = f$ with $(\mathcal{A}^{-1}f)|_{\Gamma_-} = 0$.

From (12), one sees that f_1 represents the solution with pure absorption, f_2 denotes solution after one scattering, and f_3 collects the rest.

The solution to (11), when confined on the boundary Γ_+, is the outgoing data that we measure. Let us denote it by ϕ; then

$$\phi = f|_{\Gamma_+} \quad \text{and} \quad \phi_i = f_i|_{\Gamma_+}\,, \quad i = 1,2,3\,. \tag{15}$$

Immediately,

$$\phi = \sum_{i=1}^{3} \phi_i = \mathcal{A}l[f_-]\,.$$

We now study the structure of $\mathcal{A}l$. For that we use a delta function as the incoming data for f_-, and we have the following theorem.

THEOREM 1 ([15]). *Assume that (σ, k) is admissible. Then the solution to* (1) *with*

$$f_-(x,v) = \delta(x-x')\delta(v-v'), \quad (x',v') \in \Gamma_-, \tag{16}$$

has the decomposition $f(x,v;x',v') = f_1 + f_2 + f_3$, where

$$f_1 = |n(x')\cdot v'| \int_0^{\tau_+(x',v')} e^{-\int_0^{\tau_-(x,v)} \sigma(x-sv)ds} \delta(x-x'-tv)\delta(v-v')\mathrm{d}t\,; \tag{17}$$

(18)
$$f_2 = |n(x')\cdot v'| \int_0^{\tau_-(x,v)} \int_0^{\tau_+(x',v')} e^{-\int_0^s \sigma(x-pv)dp} e^{-\int_0^{\tau_-(x-sv,v')}} \sigma(x-sv-pv',v')\mathrm{d}p \times k(x-sv,v',v)\delta(x-x'-sv-tv')\mathrm{d}t\mathrm{d}s;$$

(19) $(\min\{\tau,\lambda\})^{-1}|n(x')\cdot v'|^{-1} f_3 \in L^\infty(\Gamma_-;\mathcal{W})\,.$

Here $\lambda \geq 0$ is an arbitrary constant, and

$$\mathcal{W} = \{f : f \in L^1(\Omega\times V), v\cdot\nabla_x f \in L^1(\Omega\times V)\}\,.$$

The albedo operator only takes the information on Γ_+, and we thus write the distribution kernel $\alpha_i(x,v,x',v')$ as a confinement

$$\alpha_i(x,v;x',v') := f_i(x,v;x',v')\big|_{(x,v)\in\Gamma_+}, \quad (x',v')\in\Gamma_-\,, \qquad i=1,2,3\,.$$

It maps $(x',v')\in\Gamma_-$ to $(x,v)\in\Gamma_+$ and could be explicitly expressed as follows.

THEOREM 2 ([15]). *Assume that (σ,k) is admissible. Then $\alpha(x,v;x',v') = \alpha_1+\alpha_2+\alpha_3$, where*

(20) $$\alpha_1(x,v;x',v') = \frac{|n(x')\cdot v'|}{n(x)\cdot v} e^{-\int_0^{\tau_-(x,v)}\sigma(x-sv)\mathrm{d}s}\delta(x-x'-\tau_+(x',v')v')\delta(v-v')\,;$$

(21) $$\alpha_2(x,v;x',v') = \frac{|n(x')\cdot v'|}{n(x)\cdot v}\int_0^{\tau_+(x',v')} e^{-\int_0^{\tau_+(x'+tv',v)}\sigma(x-pv)\mathrm{d}p} e^{-\int_0^t \sigma(x+pv')\mathrm{d}p} \times k(x+tv',v',v)\delta(x-x'-tv'-\tau_+(x'+tv',v)v)\mathrm{d}t\,;$$

(22) $$\min\{\tau(x',v'),\lambda\}^{-1}|n(x')\cdot v'|^{-1}\alpha_3 \in L^\infty(\Gamma_-;L^1(\Gamma_+,\mathrm{d}\xi))\,.$$

We conclude that, for any incoming data $f_-(x,v)$,

(23) $$\phi(x,v) = \mathcal{A}l[f_-](x,v) = \sum_{i=1}^3 \phi_i = \int_{\Gamma_-}\sum_{i=1}^3 \alpha_i(x,v;x',v')f_-(x',v')\mathrm{d}\xi(x',v')\,,$$

where $\mathrm{d}\xi(x',v') = |n(x')\cdot v|\mathrm{d}\mu(x')\mathrm{d}v$ is the measure on Γ_-, and the three components have very different singularities as follows:

- α_1 is a delta function in both x and v. It is a nonnegative measure on $\Omega\times V$ and contains information only from σ and not from k.
- α_2 is an integration of a delta function over a one-dimensional manifold. The two exponentials reflect the particle traveling from x' to $x'+tv'$ and from $x'+tv'$ to x, respectively. The particle changes its velocity from v' to v at $x'+tv'$ with the probability $k(x+tv',v',v)$. This term encodes the information about particles which travel and change directions once.
- α_3 collects the rest of the information.

2.2. Discrete setting. The same formulation can be written on the discrete level. Using the notation from the introduction, we write the following equation, incorporating the boundary conditions:

(24) $$(\mathsf{I}+\mathsf{A}^{-1}\mathsf{B})\mathbf{f} = \mathsf{A}^{-1}\mathsf{J}_0\mathbf{f}_-\,,$$

where $\mathbf{f}$ is defined as in (5). Here J_0 numerically resembles $\mathcal{J}$. Denote by $N_{b\pm}$ the number of grid points (x,v) on $\Gamma_\pm$; then J_0 is a matrix of size $N_xN_v\times N_{b_-}$.

Using the Neumann expansion,

$$\begin{aligned}(\mathsf{I}+\mathsf{X})^{-1} &= \mathsf{I}-(\mathsf{I}+\mathsf{X})^{-1}\mathsf{X}\,,\\ &= \mathsf{I}-\left(\mathsf{I}-(\mathsf{I}+\mathsf{X})^{-1}\mathsf{X}\right)\mathsf{X}\\ &= \mathsf{I}-\mathsf{X}+(\mathsf{I}+\mathsf{X})^{-1}\mathsf{X}^2\,,\end{aligned}$$

we let $\mathsf{X}=\mathsf{A}^{-1}\mathsf{B}$ and separate the solution of (24) into

$$\begin{aligned}\mathbf{f} &= \mathsf{A}^{-1}\mathsf{J}_0\mathbf{f}_- - \mathsf{A}^{-1}\mathsf{B}\mathsf{A}^{-1}\mathsf{J}_0\mathbf{f}_- + (\mathsf{I}+\mathsf{A}^{-1}\mathsf{B})^{-1}(\mathsf{A}^{-1}\mathsf{B})^2\mathsf{J}_0\mathbf{f}_-\\ &:= \mathbf{f}_1+\mathbf{f}_2+\mathbf{f}_3\,.\end{aligned} \tag{25}$$

Comparing it with (12), we see that the three vectors are simply counterparts of f_i. As suggested by Theorem 1, these three vectors should have different sparsities. Similar to the discussion for the continuous setting, here we see that $\mathbf{f}_1$ includes information on A only, which could be used to recover σ, while $\mathbf{f}_2$ takes up information from B that is equivalent to Σ_k.

3. Numerical algorithm. As mentioned in the introduction, most of the currently available algorithms are based on optimization and typically are written as

$$\begin{cases} \min_{\Sigma,\Sigma_k,\{\mathbf{f}^{(i)}\}} \sum_i \|\mathsf{E}_+\mathbf{f}^{(i)}-\phi^{(i)}\| + \text{regularization}\\ \text{s.t.}\quad (\mathsf{A}+\mathsf{B})\mathbf{f}^{(i)}=\mathbf{0}\,,\quad \mathbf{f}^{(i)}\big|_{\Gamma_-}=\mathbf{f}_-^{(i)},\quad i=1,2,\dots,N_I\,,\end{cases} \tag{26}$$

where the superscript i denotes different rounds of experiments, N_I is the total number of experiments conducted, and E_+ is defined as in (8). The approach is straightforward, but it lacks analytical justification because there is no guarantee that the minimizer exists and will be unique, and it does tell us how to choose the correct regularization and what the error will be. What is more, σ and Σ_k are recovered simultaneously, which requires a lot of computation in each optimization iteration step.

In this section, we set up a new optimization framework in recovering $\sigma(x)$ and $k(x,v,v')$ *separately*. As indicated by the singular decomposition method from [15], the measurement could be separated into three parts based on the different regularities they enjoy, and the first two terms encode information for σ and k, respectively. Based on this, we propose a new recovery approach which comes with more rigorous error quantification.

3.1. Algorithm setup. We first write the algorithm in the continuous sense, following the ideas in [15]. From here on, we will assume that the experiments are well set in the sense that the measurement is placed at the boundary where free transport photons emit, corresponding to the input stimulus. Then the algorithm reads as follows.

Algorithm (continuous)
Input: concentrated source $f_-(x',v')\ \forall\ (x',v') \in \Gamma_-$; measurement $\phi(x,v)$ $\forall (x,v) \in \Gamma_+$
Output: $\sigma(x)$, $k(x,v,v')$
Step 0) Decompose data $\phi = \phi_1 + \phi_2 + \phi_3$;
Step 1) Recover $\sigma(x)$ by solving the following problem:

$$\min_{\sigma} \mathcal{F}\left(\mathcal{R}[\sigma](x,v) - a(x,v)\right)\ ; \tag{27}$$

Step 2) Recover $k(x,v,v')$ by solving

$$\begin{cases} \min_{k,f} \mathcal{F}\left(f\big|_{\Gamma_+} - \phi_1 - \phi_2\right) \\ \text{s.t. } (\mathcal{A}(\sigma) + \mathcal{B})f = 0,\ f\big|_{\Gamma_-} = f_-. \end{cases} \tag{28}$$

In the problem we formulated, $\mathcal{F}$ is a *nonnegative convex* fit-to-data function. $\mathcal{R}$ is the X-ray transform

$$\mathcal{R}[\sigma](x,v) = \int_0^{\tau_-(x,v)} \sigma(x - sv)\mathrm{d}s \quad \forall (x,v) \in \Gamma_+\,,$$

and a is calculated from the data as follows:

$$a(x,v) = \ln\left(\frac{f_-(x - \tau_-(x,v)v, v)}{\phi_1(x,v)}\right)\,. \tag{29}$$

To justify the validity of this algorithm, we note the following:

- Step 0 can be done due to the different singularities of ϕ_i according to Theorem 2, once the incoming data are made concentrated.
- Step 1 is written in an optimization form for later convenience, but in fact, the minimum could be achieved and is zero. Indeed, according to the definition in (15) and (14), one immediately sees that for all $(x,v) \in \Gamma_+$, given $x - x' /\!/ v$ and $v = v'$,

$$\mathcal{R}[\sigma](x,v) = \int_0^{\tau_-(x,v)} \sigma(x - sv)\mathrm{d}s = \ln\left[f_-(x',v')/\phi_1(x,v)\right]\,, \tag{30}$$

  which is the same as $a(x,v)$ in (29).
- Step 2 is also written in the optimization form. From the theory in [15], a unique recovery of k is available once σ_a is obtained from the first step. Therefore, the minimum could be achieved and is zero.

Remark 1. Another straightforward solver is to replace the optimization problem in Step 1 by

$$\begin{cases} \min_{\sigma,f} \mathcal{F}\left(f\big|_{\Gamma_+} - \phi_1\right) \\ \text{s.t. } \mathcal{A}f = 0,\ f\big|_{\Gamma_-} = f_-. \end{cases} \tag{31}$$

However, as we can see, σ here is involved in a nonlinear way, making the optimization problem harder to analyze.

The same procedure could be taken in the discrete setting for numerical simulation.

Algorithm (discrete)

Input: concentrated source $\mathbf{f}_-^{(i)}$, concentrating around $(x^{(i)}, v^{(i)}) \in \Gamma_-$; measurement $\phi^{(i)}$. $i = 1, \ldots, N_I$.

Output: Σ, Σ_k

Step 0) Decompose data $\phi^{(i)} = \phi_{R,1}^{(i)} + \phi_{R,2}^{(i)} + \phi_{R,3}^{(i)} \quad \forall i$;

Step 1) Recover Σ by solving the following problem:

$$\min_{\Sigma} \mathcal{F}\left(\mathsf{R} \cdot \Sigma - \mathbf{a}\right); \tag{32}$$

Step 2) Recover Σ_k by solving

$$\begin{cases} \min_{\Sigma_k, \{\mathbf{f}^{(i)}\}} \mathcal{F}\left(\left\{\mathsf{E}_+ \mathbf{f}^{(i)} - \phi_1^{(i)} - \phi_2^{(i)}\right\}_{i=1,2,\ldots,N_I}\right) \\ \text{s.t. } (\mathsf{A}(\Sigma) + \mathsf{B})\mathbf{f}^{(i)} = 0, \quad \mathbf{f}^{(i)}\big|_{\Gamma_-} = \mathbf{f}_-^{(i)}, \quad i = 1, 2, \ldots, N_I. \end{cases} \tag{33}$$

Here the subindex R in Step 0 indicates the numerical recovery. $\mathcal{F}$ is the discrete version of the fit-to-data function, and R is the numerical integration of the X-ray transform in (30), with each of its rows representing one experiment. Vector $\mathbf{a}$ consists of data collected at a specific grid point as follows:

$$\mathbf{a}_j = \ln\left(\frac{\mathbf{f}_-^{(j)}(x^{(j)}, v^{(j)})}{\phi_{R,1}^{(j)}(x_*^{(j)}, v_*^{(j)})}\right), \tag{34}$$

where $(x^{(j)}, v^{(j)}) \in \Gamma_-$, and its counterpart denoted as $(x_*^{(j)}, v_*^{(j)})$ takes the form

$$x_*^{(j)} = x^{(j)} + \tau_+(x^{(i)}, v^{(i)})v^{(i)}, \quad v_*^{(j)} = v^{(j)}. \tag{35}$$

As written, these steps are identical to those of the algorithm in the continuous setting, and each step requires a specially designed implementation to ensure the well-posedness and controllable error. We discuss the implementation in the following subsection, and the error analysis is left to section 4.

Remark 2. An immediate advantage of our new formulation (32) over the conventional one (26) is the size reduction: instead of looking for Σ and Σ_k simultaneously, which is a problem of size $(N_x N_v + N_x)^2$, we find Σ first and then find Σ_k, and the former is of a much reduced size.

3.2. Implementation. In this section, we will make clear how each of those steps in the discrete algorithms can be performed.

3.2.1. Decomposition. Given concentrated incoming data $f_-^{(i)}$ on Γ_-, one could collect the outgoing data $\phi^{(i)}$ on Γ_+, which analytically can be separated into three parts $\phi_{1/2/3}^{(i)}$. Numerically, however, it is not possible to conduct the separation exactly. Instead, we obtain the recovered data, denoted as $\phi_{R,1/2/3}^{(i)}$. Therefore, we need to find a simple way to define $\phi_{R,j}^{(i)}$ so that it is close enough to $\phi_j^{(i)}$ with a small error. To this end, let us first assume that $f_-^{(i)}$ is concentrated around $(x^{(i)}, v^{(i)})$, with the width smaller than Δx and Δv. Therefore, $\mathbf{f}_-^{(i)}$ has only one nonzero value located at $(x^{(i)}, v^{(i)})$ grid. Then we simply set

(36)

$$\phi_{R,1}^{(i)}(x,v) = \begin{cases} \phi(x,v)\,, & x = x_*^{(i)},\ v = v_*^{(i)}, \\ 0 & \text{elsewhere,} \end{cases} \qquad (x^{(i)}, v^{(i)}) \in \Gamma_-, \quad (x_*^{(i)}, v_*^{(i)}) \in \Gamma_+\,;$$

$$\phi_{R,2}^{(i)}(x,v) = \begin{cases} \phi(x,v)\,, & \exists (s,t) \text{ s.t. } x - sv = x^{(i)} + tv^{(i)}, \quad v \neq v^{(i)}, \\ 0 & \text{elsewhere;} \end{cases}$$

$$\phi_{R,3}^{(i)} = \phi - \phi_{R,1} - \phi_{R,2}\,.$$

3.2.2. Recovering Σ. To recover σ from ϕ_1, one just needs to conduct an inverse X-ray transform as displayed in (30). Since the X-ray transform has an explicit inversion formula (which will be detailed below) and is in integral form, one way to do this in the discrete setting is to use quadrature rules to approximate the inversion formula. This requires evaluating the integrand on the grids and performing the summation. However, the process is well known to be numerically very unstable [10, 28]. To overcome this difficulty, many strategies have been invented, including the algebraic reconstruction technique and direct algebraic methods, among many others [28]. In the early 2000s, more attention was placed on using the optimization framework instead of employing a direct inversion along with adopting Tikhonov regularization to overcome large conditioning. This is the approach that we will be taking.

Specifically, in Step 1 we modify the optimization with a regularizer:

$$\min_{\Sigma} \|\mathsf{R}\cdot\Sigma - \mathbf{a}\|_X + \lambda\|\Sigma\|_Y\,, \tag{37}$$

where the first term represents the mismatch and the second term is the regularizer ensuring that the error in the measurement stays controlled. Both terms are convex, and existence and uniqueness of the minimizer are obvious. Note that we do not pick a specific optimization algorithm here. The performance of varying optimization algorithms could be drastically different. In recent years it was discovered that stochastic optimization advances the traditional method, and it has been used in optical tomography for recovering coefficients in RTE [11]. We omit the discussion here. In the next section, we will analyze the error brought about by the introduction of the regularizer.

We remark here that a more straightforward form in recovering σ in our problem could be

$$\begin{cases} \min_{\sigma, \{\mathbf{f}^{(i)}\}} \sum_{i=1}^{N_I} \|\mathsf{E}_+\mathbf{f}^{(i)} - \phi_1^{(i)}\|_X + \lambda\|\sigma\|_Y \\ \text{s.t. } \mathsf{A}\mathbf{f}^{(i)} = 0, \quad \mathbf{f}^{(i)}\big|_{\Gamma_-} = \mathbf{f}_-^{(i)}\,, \quad i = 1, 2, \ldots, N_I\,, \end{cases}$$

which can be considered as a numerical implementation of (31). However, as claimed before, here σ is involved in the problem in a nonlinear fashion, and it is not clear why the minimizer exists, or is unique, and the error would be hard to quantify.

To end this section, we include the inversion formula for the X-ray transform for completeness. In 2D ($x, v \in \mathbb{R}^2$), the X-ray transform is equivalent to the Radon transform, which admits the following unique inversion formula [9]:

$$\sigma(x) = \frac{1}{2\pi^2}\int_0^\pi \mathcal{R}[\sigma(\cdot,\theta) * h](x_1\cos\theta + x_2\sin\theta)\mathrm{d}\theta\,. \tag{38}$$

Here h is the inverse Fourier transform of $|k|$, and $\mathcal{R}[\sigma]$ is defined as in (30). For dimension higher than two, the X-ray transform is different from the Radon transform,

and one needs to first translate a series of X-ray projections into a Radon projection and then perform the inverse Radon transform [18, 19, 20]. Specifically, for helical source trajectories, denote

$$\mathcal{D}(y,v)=\int_0^{\tau_-(y,v)}\sigma(y-sv)\mathrm{d}s\,,$$

and then for a properly chosen vector $e_\nu(p,x)$ and weight μ_ν, the reconstruction formula is

$$\sigma(x)=-\frac{1}{2\pi}\int_{I_{BP}(x)}\frac{I(p,x)}{|x-y(p)|}\mathrm{d}p\,, \tag{39}$$

where

$$I(p,x)=\sum_\nu^{N_e}\mu_\nu\int_{-\pi}^{\pi}\mathcal{D}'(y(p),\cos\gamma b+sin\gamma e_\mu)\frac{1}{\sin\gamma}\mathrm{d}\gamma\,,$$

and the derivative of $\mathcal{D}$ is with respect to the first variable. $I_{BP}(x)$ is the back-projection interval [9]. Here, in either case, we see that analytically a unique reconstruction of $\sigma(x)$ is available.

4. Error analysis. This section is devoted to analyzing the reconstruction error $\|\Sigma-\sigma_a^{dis}\|_2$, where Σ is obtained from solving (37) with $\phi_{R,1}$ given in (36). σ_a^{dis} is the true media sampled on the grid points, with the superscript "dis" indicating that it is the discrete version. The analysis below is confined in three dimensions.

In the recovery for Σ, two steps are taken: the separation of data and the minimization for the inverse X-ray transform. We cumulatively analyze them as follows:

(1) Data separation: to extract $\phi_1^{(i)}$ from the measurement $\phi^{(i)}$, some assumptions have been made, and we need to study $\|\phi_{R,1}^{(i)}-\phi_1^{(i)}\|$, the distance between the recovery (36) and the true data.
(2) Determine Σ from (37) using the discrete reconstruction formula. The regularization has been added to control the error from (1), but it inevitably introduces the regularizing error.

We examine each error closely in the following two subsections.

4.1. Study of $\phi_{R,1}-\phi_1$. According to (36), incoming data are placed at (x_0,v_0), and $\phi_{R,1}$ is defined as zero except for the particular point $(x_0+\tau_+(x_0,v_0)v_0,v_0)$ which is the counterpart of (x_0,v_0) on Γ_+, and at this point, $\phi_{R,1}$ simply takes the value of ϕ, with the intuition that both ϕ_2 and ϕ_3 make very limited contributions at this particular point. In this section we quantify the error produced by ignoring $\phi_{2/3}$'s contribution.

More precisely, assume that the incoming source $f_-(x',v')=\psi(\frac{|x'-x_0|}{\varepsilon})\psi(\frac{|v'-v_0|}{\varepsilon})$ is concentrated at $(x_0,v_0)\in\Gamma_-$ and that the measurement is taken in the neighborhood of its counterpart coordinate $(x_{0*},v_{0*}):=((x_0+\tau_+(x_0,v_0)v_0,v_0)\in\Gamma_+$, i.e.,

$$E_i=\int_{\Gamma_+}\phi_i(x,v)\psi\left(\frac{|x-(x_0+\tau_+(x_0,v_0)v_0)|}{\varepsilon_1}\right)\psi\left(\frac{|v-v_0|}{\varepsilon_1}\right)\mathrm{d}\xi(x,v)\,.$$

Here ε and ε_1 denote the concentration of the source and measurement, respectively. ψ is a smooth positive function supported on $[-1,1]$ with $\psi=1$ on $[-1/2,1/2]$. Then

using (23), E_i reads

(40)
$$E_i = \int_{\Gamma_-}\int_{\Gamma_+} \alpha_i(x,v;x',v')\psi\left(\frac{|x'-x_0|}{\varepsilon}\right)\psi\left(\frac{|v'-v_0|}{\varepsilon}\right) \psi\left(\frac{|x-(x_0+\tau_+(x_0,v_0)v_0)|}{\varepsilon_1}\right)\psi\left(\frac{|v-v_0|}{\varepsilon_1}\right)\mathrm{d}\xi(x,v)\mathrm{d}\xi(x',v')\,.$$

We will show that E_1 is much larger than $E_{2,3}$ for small ε and ε_1, which implies that, at this particular point, the error $\phi_{R,1}-\phi_1=\phi-\phi_1=\phi_2+\phi_3$ is small. In particular, we have the following.

THEOREM 3. *Consider the incoming data given by* $f_-(x',v')=\psi(\frac{|x'-x_0|}{\varepsilon})\psi(\frac{|v'-v_0|}{\varepsilon})$ *and by* E_i *defined in* (40). *Assume there exist positive constants* C_1 *such that*

$$\sigma(x)\le C_1,\quad k(x,v,v')\le C_1\quad \forall x,v,v'\,,$$

and τ_+ *is Lipschitz continuous near* (x_0,v_0). *Then there exist constants* c, C, *and* C_δ *such that*

$$E_1\ge c\varepsilon_1^4,\quad E_2\le C\varepsilon^4\varepsilon_1^2,\quad E_3\le C_\delta\varepsilon_1^{2-\delta}\varepsilon^4$$

for any $\delta>0$. *Consequently, we have*

$$\frac{E_2+E_3}{E_1}=\mathcal{O}(\varepsilon_1^{-2-\delta}\varepsilon^4)\quad \textit{for any}\ \ \delta>0\,, \tag{41}$$

and thus the relative error is

$$\frac{|\phi_{R,1}-\phi_1|}{|\phi_1|}=O(\varepsilon_1^{-2-\delta}\varepsilon^4). \tag{42}$$

To get the relationship among the E_i's, we need to estimate their magnitudes individually. From the relation (40) and the expression of α_1 and α_2 in (20) and (22), E_1 and E_2 can be evaluated straightforwardly. On the contrary, E_3 needs more sophisticated analysis, and as such we first bound α_3, the kernel of the third part of the albedo operator, in the following proposition.

PROPOSITION 1. $\alpha_3(x,v;x',v')\in L^\infty(\Gamma_-,L^p(\Gamma_+,\mathrm{d}\xi))$ *if* $p<2$.

To prove this theorem, notice that $\alpha_3=f_3\big|_{(x,v)\in\Gamma_+}$, $f_3=(\mathcal{A}^{-1}\mathcal{B})^2 f$, and by Proposition 2.3 of [15], $\|f\|_{L^1(\Omega\times V)}\le C\|f_-\|_{L^1(\mathrm{d}\xi)}$; therefore we basically need the boundedness of $\mathcal{A}^{-1}$ and $\mathcal{B}\mathcal{A}^{-1}\mathcal{B}$ (Lemmas 1 and 2). We will also show that the operator $\mathcal{B}\mathcal{A}^{-1}\mathcal{B}$ could send L^1 data to L^p (Lemma 4). The results are summarized in Lemmas 1–4.

LEMMA 1. *Let* g *be a function defined on* $\Omega\times V$, *and let* $1\le p<\infty$. *Then* $\exists C$ *such that*

$$\|\mathcal{A}^{-1}g|_{\Gamma_+}\|_{L^p(\mathrm{d}\xi)}\le C\|g\|_{L^p(\Omega\times V)}.$$

Proof.

$$\begin{aligned}\|\mathcal{A}^{-1}g|_{\Gamma_+}\|^p_{L^p(\mathrm{d}\xi)} &= \int_{\Gamma_+}\left|\int_0^{\tau_-(x,v)} e^{-\int_0^t \sigma(x-sv,v)\mathrm{d}s} g(x-tv,v)\mathrm{d}t\right|^p \mathrm{d}\xi(x,v)\\ &\le \int_{\Gamma_+}\left[\int_0^{\tau_-(x,v)} |g(x-tv,v)|\mathrm{d}t\right]^p \mathrm{d}\xi(x,v)\\ &\le C\int_{\Gamma_+}\int_0^{\tau_-(x,v)} |g(x-tv,v)|^p \mathrm{d}t\mathrm{d}\xi(x,v)\\ &= C\|g\|^p_{L^p(X\times V)},\end{aligned}$$

where the second inequality uses the Hölder inequality, and $C = \sup_{x,v}\tau_-(x,v)^{p/p'}$, $\frac{1}{p}+\frac{1}{p'}=1$. ∎

LEMMA 2. *Let g be a function defined on $\Omega\times V$. Assume that $k(x,v,v')\le C_1$. If $p\ge 1$ and $q<\frac{3p}{3-p}<\infty$, then*

$$\|\mathcal{B}\mathcal{A}^{-1}\mathcal{B}g\|_{L^q(\Omega\times V)} \le C(p,q)\|g\|_{L^p(\Omega\times V)}.$$

Proof.

(43)

$$\begin{aligned}(\mathcal{B}\mathcal{A}^{-1}\mathcal{B}g)(x,v) &= -\int_V k(x,v',v)\int_0^{\tau_-(x,v')} e^{-\int_0^t\sigma(x-sv')\mathrm{d}s}(\mathcal{B}g)(x-tv',v')\mathrm{d}t\mathrm{d}v'\\ &= -\int_{\Omega_x} k(x,v',v)e^{-\int_0^t\sigma(x-sv')\mathrm{d}s}(\mathcal{B}g)(y,v')t^{-2}\mathrm{d}y\\ &= -\int_{\Omega_x} k(x,v',v)e^{-t\int_0^1\sigma((1-s')x+s'y)\mathrm{d}s'}\int_V k(y,w,v')g(y,w)\mathrm{d}w t^{-2}\mathrm{d}y\\ &= \int_\Omega\int_V K_1(x,v,y,w)g(y,w)\mathrm{d}w\mathrm{d}y,\end{aligned}$$

with the change of variable

$$y = x-tv',\quad \mathrm{d}y = t^2\mathrm{d}t\mathrm{d}v',\quad t=|x-y|,\quad v' = \frac{x-y}{|x-y|},$$

and Ω_x, the integration domain of y, is the set of $y\in\Omega$ such that the segment from x to y is contained in Ω.

The integral kernel K_1 is given by

$$K_1(x,v,y,w) = \mathbf{1}_{\Omega_x}(y)k(x,v',v)e^{-t\int_0^1\sigma((1-s')x+s'y)\mathrm{d}s'}k(y,w,v')|x-y|^{-2}.$$

Thus, by the assumption that $k\in L^\infty$, one has

$$|K_1(x,v,y,w)|\le C|x-y|^{-2}. \tag{44}$$

Using this estimate, we can finish the proof by the Hardy–Littlewood–Sobolev (HLS)

inequality as follows:

$$\begin{aligned}\|\mathcal{B}\mathcal{A}^{-1}\mathcal{B}g\|^q_{L^q(X\times V)} &\le C\|\,|x|^{-2} *_{x,v} g\|^q_{L^q(X\times V)}\\ &= C\int_{\Omega\times V}\left|\int_{\Omega\times V}|x-y|^{-2}g(y,w)\mathrm{d}y\mathrm{d}w\right|^q \mathrm{d}x\mathrm{d}v\\ &\le C\int_{\Omega}\left|\int_{\Omega}|x-y|^{-2}\tilde{g}(y)\mathrm{d}y\right|^q \mathrm{d}x\\ &= C\|\,|x|^{-2} *_x \tilde{g}\|^q_{L^q(\Omega)}\\ &\le C\|\tilde{g}\|^q_{L^p(\Omega)}\,,\end{aligned}$$

where $\tilde{g}(x) = \int_V g(x,v)\mathrm{d}v$, and the last inequality uses the HLS inequality in Ω, hereby imposing the restrictions on p and q. Then notice from the Hölder inequality that

$$\|\tilde{g}\|^p_{L^p(\Omega)} = \int_\Omega\left|\int_V g(x,v)\mathrm{d}v\right|^p \mathrm{d}x \le C\int_\Omega\int_V |g|^p\mathrm{d}v\mathrm{d}x = C\|g\|^p_{L^p(\Omega\times V)}\,,$$

and the result directly follows. ∎

LEMMA 3. *Let f_1 be defined as in* (17)*; then for $p<2$,*

$$\|\mathcal{B}\mathcal{A}^{-1}\mathcal{B}f_1\|_{L^p(\Omega\times V)} \le C_p\,.$$

Proof. Recall f_1,

$$f_1(x,v) = |n(x')\cdot v'|\int_0^{\tau_+(x',v')} e^{-\int_0^{\tau_-(x,v)}\sigma(x-sv)\mathrm{d}s}\delta(x-x'-tv)\delta(v-v')\mathrm{d}t\,.$$

Then

$$\begin{aligned}|\mathcal{B}\mathcal{A}^{-1}\mathcal{B}f_1(x,v)| &\le C\int_\Omega\int_V\int_0^{\tau_+(x',v')}|x-y|^{-2}\delta(y-x'-tw)\delta(w-v')\mathrm{d}t\mathrm{d}w\mathrm{d}y\\ &= C\int_0^{\tau_+(x',v')}|x-(x'+tv')|^{-2}\mathrm{d}t\end{aligned}$$

thanks to (43) and (44).

For any $x\in X$, write the parallel and perpendicular components of $x-x'$ with respect to v' as

$$x = x' + x_\parallel + x_\perp,\quad \text{with}\quad x_\parallel = ((x-x')\cdot v')v'\,,$$

and then one sees that

$$\begin{aligned}\int_{-\infty}^{\infty}|x-(x'+tv')|^{-2}\mathrm{d}t &= \int_{-\infty}^{\infty}(|x_\parallel - tv'|^2+|x_\perp|^2)^{-1}\mathrm{d}t = \int_{-\infty}^{\infty}(|x_\parallel - t|^2+|x_\perp|^2)^{-1}\mathrm{d}t\\ &= \int_{-\infty}^{\infty}(|t|^2+|x_\perp|^2)^{-1}\mathrm{d}t = \pi|x_\perp|^{-1}\,.\end{aligned}$$

Therefore, for any $q < 2$,

$$\|\mathcal{B}\mathcal{A}^{-1}\mathcal{B}f_1\|_{L^q}^q \le C\int_\Omega\int_V |x_\perp|^{-q}\mathrm{d}v\mathrm{d}x = C\int_{-R}^{R}\int_{|x_\perp|\le R}|x_\perp|^{-q}\mathrm{d}x_\perp\mathrm{d}|x_\parallel| \le C\,,$$

where R is the diameter of Ω, since $x_\perp$ lives in a 2D space. ∎

LEMMA 4. *Let f be the solution to* (1) *with incoming data* (16)*; then for $p < 2$ there is C such that $\|\mathcal{B}\mathcal{A}^{-1}\mathcal{B}f\|_{L^p(\Omega\times V)} \le C$.*

Proof. From the previous lemma, we know that $\|\mathcal{B}\mathcal{A}^{-1}\mathcal{B}f_1\|_{L^p(\Omega\times V)} \le C$ for any $p < 2$. Then notice that $\mathcal{A}^{-1}$ and $\mathcal{B}$ are bounded operators on L^p (which is obvious from their explicit expressions). Then, since $\mathcal{B}\mathcal{A}^{-1}\mathcal{B}f_2 = -\mathcal{B}\mathcal{A}^{-1}\mathcal{B}(\mathcal{A}^{-1}\mathcal{B}f_1) = -\mathcal{B}\mathcal{A}^{-1}(\mathcal{B}\mathcal{A}^{-1}\mathcal{B}f_1)$, one gets $\|\mathcal{B}\mathcal{A}^{-1}\mathcal{B}f_2\|_{L^p(\Omega\times V)} \le C$. Finally, from the fact that $\|f\|_{L^1(\Omega\times V)} \le C$, one gets $\|f_3\|_{L^q(\Omega\times V)} = \|\mathcal{A}^{-1}\mathcal{B}\mathcal{A}^{-1}\mathcal{B}f\|_{L^q(\Omega\times V)} \le C$ by Lemma 2 if $q < 3/2$. Then using Lemma 2 again gives $\|\mathcal{B}\mathcal{A}^{-1}\mathcal{B}f_3\|_{L^p(\Omega\times V)} \le C$ for any $p < 3$. ∎

Finally, given the fact that $f_3 = (\mathcal{A}^{-1}\mathcal{B})^2 f$, Lemmas 1 and 4 imply Proposition 1. The proof of Theorem 3 is now in order.

Proof of Theorem 3. Using (20), one can see that

$$\begin{aligned}
E_1 = &\int_{\Gamma_-}\int_{\Gamma_+}\frac{|n(x')\cdot v'|}{n(x)\cdot v}e^{-\int_0^{\tau_-(x,v)}\sigma(x-sv)ds}\delta(x-x'-\tau_+(x',v')v')\delta(v-v')\\
&\psi\left(\frac{|x'-x_0|}{\varepsilon}\right)\psi\left(\frac{|v'-v_0|}{\varepsilon}\right)\psi\left(\frac{|x-(x_0+\tau_+(x_0,v_0)v_0)|}{\varepsilon_1}\right)\\
&\psi\left(\frac{|v-v_0|}{\varepsilon_1}\right)\mathrm{d}\xi(x,v)\mathrm{d}\xi(x',v')\\
= &\int_{\Gamma_-}|n(x')\cdot v'|e^{-\int_0^{\tau_-((x'+\tau_+(x',v')v'),v')}\sigma((x'+\tau_+(x',v')v')-pv')\mathrm{d}p}\\
&\psi\left(\frac{|x'-x_0|}{\varepsilon}\right)\psi\left(\frac{|v'-v_0|}{\varepsilon}\right)\\
&\psi\left(\frac{|(x'+\tau_+(x',v')v')-(x_0+\tau_+(x_0,v_0)v_0)|}{\varepsilon_1}\right)\psi\left(\frac{|v'-v_0|}{\varepsilon_1}\right)\mathrm{d}\xi(x',v')\,.
\end{aligned}\tag{45}$$

Due to the Lipschitz continuity of τ_+, there exists a small constant $c < \frac{1}{2}$ such that $|x'-x_0| < c\varepsilon_1, |v'-v_0| < c\varepsilon_1$ implies $|(x'+\tau_+(x',v')v') - (x_0+\tau_+(x_0,v_0)v_0)| < \frac{1}{2}\varepsilon_1$. Also, since τ_- and σ have upper bounds, the exponential term has a lower bound. Thus,

$$|E_1| \ge \int_{|x'-x_0|<c\varepsilon_1,|v'-v_0|<c\varepsilon_1}\mathrm{d}\xi(x',v') \ge c\varepsilon_1^4\,.$$

To estimate E_2, one uses (22) to get

$$
\begin{aligned}
|E_2| = & \int_{\Gamma_-}\int_{\Gamma_+}\int_0^{\tau_+(x',v')} \frac{|n(x')\cdot v'|}{n(x)\cdot v} \\
& e^{-\int_0^{\tau_+(x'+tv',v)}\sigma(x-pv)dp} e^{-\int_0^t \sigma(x+pv')dp} k(x+tv',v',v) \\
& \delta(x-x'-tv'-\tau_+(x'+tv',v))\mathrm{d}t\psi\left(\frac{|x'-x_0|}{\varepsilon}\right)\psi\left(\frac{|v'-v_0|}{\varepsilon}\right) \\
& \psi\left(\frac{|x-(x_0+\tau_+(x_0,v_0)v_0)|}{\varepsilon_1}\right)\psi\left(\frac{|v-v_0|}{\varepsilon_1}\right)\mathrm{d}\xi(x,v)\mathrm{d}\xi(x',v') \\
\leq\ & C\sup_t \int_{\Gamma_-}\int_V \frac{|n(x')\cdot v'||n(x'+tv'+\tau_+(x'+tv',v)v)\cdot v|}{n(x'+tv'+\tau_+(x',+tv',v)v)\cdot v}\psi\left(\frac{|x'-x_0|}{\varepsilon}\right) \\
& \psi\left(\frac{|v'-v_0|}{\varepsilon}\right)\psi\left(\frac{|(x'+tv'+\tau_+(x'+tv',v)v)-(x_0+\tau_+(x_0,v_0)v_0)|}{\varepsilon_1}\right) \\
& \psi\left(\frac{|v-v_0|}{\varepsilon_1}\right)\mathrm{d}v\mathrm{d}\xi(x',v') \\
\leq\ & C\int_{|x'-x_0|<\varepsilon,|v'-v_0|<\varepsilon,|v-v_0|<\varepsilon_1} \mathrm{d}v\mathrm{d}\xi(x',v') \leq C\varepsilon^4\varepsilon_1^2\,,
\end{aligned}
$$

where in the first inequality we bound the exponential terms and the k term by C and then integrate out the x variable.

For E_3, we have

$$
\begin{aligned}
|E_3| \leq & \int_{|x'-x_0|<\varepsilon,|x-(x_0+\tau_+(x_0,v_0)v_0|<\varepsilon_1,|v'-v_0|<\varepsilon,|v-v_0|<\varepsilon_1} \alpha_3(x,v;x',v')\mathrm{d}\xi(x,v)\mathrm{d}\xi(x',v') \\
\leq & \int_{|x'-x_0|<\varepsilon,|v'-v_0|<\varepsilon} \|\alpha_3(\cdot,\cdot;x',v')\|_{L^p(\mathrm{d}\xi)} \\
& \|\mathbf{1}_{|x-(x_0+\tau_+(x_0,v_0)v_0|<\varepsilon_1,|v-v_0|<\varepsilon_1}\|_{L^{p'}(\mathrm{d}\xi)}\mathrm{d}\xi(x',v') \\
\leq & C_p\varepsilon^{4/p'}\int_{|x'-x_0|<\varepsilon,|v'-v_0|<\varepsilon}\mathrm{d}\xi(x',v') \\
\leq & C_p\varepsilon_1^{4/p'}\varepsilon^4
\end{aligned}
$$

thanks to Proposition 1 and the Hölder inequality. Notice that $4/p' = 2-\delta$ if $p = \frac{2}{1+\delta/2} < 2$, and (41) directly follows. To go from (41) to (42), one just needs to notice that $\phi_1 = \lim_{\varepsilon\to 0,\varepsilon_1\to 0} E_1$ and $\phi_{R,1} = \lim_{\varepsilon\to 0,\varepsilon_1\to 0} E$. ∎

4.2. Study of $\Sigma - \sigma$. We study the error in the final recovery. Comparing (27) and (37), we see that the true media σ minimizes,

$$\min_\sigma \mathcal{F}\left(\mathcal{R}[\sigma](x,v) - a(x,v)\right)\,,$$

or directly,

$$\mathcal{R}[\sigma](x,v) = a(x,v)\,,$$

while the numerical recovery Σ satisfies

$$\min_\Sigma \|\mathsf{R}\cdot\Sigma - \mathbf{a}\|_X + \lambda\|\Sigma\|_Y\,,$$

with a and $\mathbf{a}$ defined as in (29) and (34), respectively.

The difference between $\mathcal{R}[\sigma]$ and $\mathsf{R}\cdot\Sigma$ is governed by the accuracy of the quadrature rule. Suppose the second order trapezoidal rule is used to approximate the line integral of $\mathcal{R}$, and then the truncation error is given by, for each experiment,

$$\mathcal{R}[\sigma](x^{(k)},v^{(k)}) - (\mathsf{R}\cdot\sigma_a^{\rm dis})_k = \mathcal{O}(\Delta x^2)\,. \tag{46}$$

The difference between a and $\mathbf{a}$, according to the definition, is due to the error in ϕ_1.

LEMMA 5. *With incoming data given by* $f_-(x',v') = \psi(\frac{|x'-x^{(j)}|}{\varepsilon})\psi(\frac{|v'-v^{(j)}|}{\varepsilon})$, *the analytical* $a(x,v)$ *and the discrete* $\mathbf{a}$ *differ by* $\mathcal{O}(\varepsilon_1^{-2-\delta}\varepsilon^4)$ *(with arbitrary small* $\delta>0$*), i.e.,*

$$a(x_*^{(j)},v_*^{(j)}) - \mathbf{a}_j = \ln\left(\frac{f_-(x^{(j)},v^{(j)})}{\phi_1(x_*^{(j)},v_*^{(j)})}\right) - \ln\left(\frac{\mathbf{f}_-(x^{(j)},v^{(j)})}{\phi_{R,1}(x_*^{(j)},v_*^{(j)})}\right) = \mathcal{O}(\varepsilon_1^{-2-\delta}\varepsilon^4)\,,$$

where $(x^{(j)},v^{(j)})\in\Gamma_-$, *and* $(x_*^{(j)},v_*^{(j)})\in\Gamma_+$ *is defined as in* (35)*, and both are on the grid points.*

Proof. It is an immediate consequence of Theorem 3 and the definition of a. ∎

We then have the following theorem.

THEOREM 4. *If the norms in* (37) *are both taken as the* L^2 *norm and assume the range condition, then there exists a vector* z *such that*

$$\sigma^{dis} = \mathsf{R}^T z\,. \tag{47}$$

Then by choosing

$$\lambda = \frac{\varepsilon_1^{-2-\delta}\varepsilon^4 + \Delta x^2}{\|z\|_2} \tag{48}$$

in (37) *with* $\delta>0$*, one has the error estimate*

$$\|\Sigma - \sigma^{dis}\|_2 \le C\|z\|_2^{1/2}(\varepsilon_1^{-2-\delta}\varepsilon^4 + \Delta x^2)^{1/2}\,. \tag{49}$$

Proof. The major part of the proof follows a standard result from Tikhonov regularization, as summarized in [35, 17]. First, according to Lemma 5 and (46), one has

$$\mathbf{a} = a(x,v) + \mathcal{O}(\varepsilon_1^{-2-\delta}\varepsilon^4) = \mathsf{R}\cdot\sigma^{dis} + \mathcal{O}(\varepsilon_1^{-2-\delta}\varepsilon^4 + \Delta x^2)\,,$$

and thus,

$$\mathsf{R}\cdot\sigma^{dis} = \mathbf{a} + C\left(\varepsilon_1^{-2-\delta}\varepsilon^4 + \Delta x^2\right)\,. \tag{50}$$

If we consider the L^2 norm, i.e., (37) reads

$$\min_{\Sigma}\|\mathsf{R}\cdot\Sigma - \mathbf{a}\|_2^2 + \lambda\|\Sigma\|_2^2\,,$$

then the minimizer Σ reads

$$\Sigma = (\mathsf{R}^T\mathsf{R} + \lambda\mathsf{I})^{-1}\mathsf{R}^T\mathbf{a}\,. \tag{51}$$

Comparing (50) and (51), we see that their error can be computed as

$$\begin{aligned}\Sigma - \sigma^{dis} &= (\mathsf{R}^T\mathsf{R} + \lambda \mathsf{I})^{-1}\mathsf{R}^T\mathsf{R}\sigma^{dis} - \sigma^{dis} - (\mathsf{R}^T\mathsf{R} + \lambda \mathsf{I})^{-1}\mathsf{R}^T C(\varepsilon_1^{-2-\delta}\varepsilon^4 + \Delta x^2)\\ &= \left[(\mathsf{R}^T\mathsf{R} + \lambda \mathsf{I})^{-1}\mathsf{R}^T\mathsf{R}\sigma^{dis} - \sigma^{dis}\right] - (\mathsf{R}^T\mathsf{R} + \lambda \mathsf{I})^{-1}\mathsf{R}^T C(\varepsilon_1^{-2-\delta}\varepsilon^4 + \Delta x^2)\\ &= e^{reg} + e^{qua}\,,\end{aligned}$$

where the first part e^{reg} is the regularization error, and the second e^{qua} is the error from computing $\mathbf{a}$ and may get amplified in the optimization process.

Now write the singular value decomposition of $\mathsf{R} = U\Lambda V^T$, and denote the columns of U and V as u_i and v_i, respectively, and the elements in Λ as s_i. Then we have

$$\begin{aligned}\|e^{qua}\|_2 &= \left\|\sum_i v_i (s_i^2 + \lambda)^{-1} s_i u_i^T C(\varepsilon_1^{-2-\delta}\varepsilon^4 + \Delta x^2)\right\|_2\\ &\le \frac{C}{\sqrt{\lambda}}(\varepsilon_1^{-2-\delta}\varepsilon^4 + \Delta x^2)\,,\end{aligned} \tag{52}$$

where we have used the Cauchy–Schwarz inequality and the fact that $s_i/(s_i^2+\lambda) \le \frac{1}{\sqrt{\lambda}}$ to get the inequality. For e^{reg}, using the range condition (47), we have

$$e^{reg} = \sum_i v_i \frac{-\lambda}{s_i^2 + \lambda} s_i (u_i^T z)\,,$$

and therefore,

$$\|e^{reg}\| = \sum_i \left(\frac{\lambda s_i}{\lambda + s_i^2}\right)(u_i^T z)^2 \le \|z\|_2^2 \max_i \left(\frac{\lambda s_i}{\lambda + s_i^2}\right)^2 \le C\lambda \|z\|_2^2\,. \tag{53}$$

Combining (53) and (52), we have

$$\|\Sigma - \sigma^{dis}\|_2 \le C\left(\sqrt{\lambda}\|z\|_2 + \frac{1}{\sqrt{\lambda}}(\varepsilon_1^{-2-\delta}\varepsilon^4 + \Delta x^2)\right);$$

then choosing λ from (48), we see that the result (49) directly follows. ∎

Using the same idea, we give an estimate for the sensitivity of the recovery of σ on the measurement error of $\phi_{R,1}$.

COROLLARY 1. *Assume that the measurement of $\phi_{R,1}(x_*^{(j)}, v_*^{(j)})$ has an error up to $\varepsilon_m > 0$, being sufficiently small. Then, under the condition* (47) *and choosing*

$$\lambda = \frac{\varepsilon_1^{-2-\delta}\varepsilon^4 + \varepsilon_m + \Delta x^2}{\|z\|_2}\,, \tag{54}$$

one has the error estimate

$$\|\Sigma - \sigma^{dis}\|_2 \le C\|z\|_2^{1/2}(\varepsilon_1^{-2-\delta}\varepsilon^4 + \varepsilon_m + \Delta x^2)^{1/2}\,. \tag{55}$$

Proof. Denote $\tilde{\phi}_{R,1}(x_*^{(j)}, v_*^{(j)})$ as the measurement of $\phi_{R,1}(x_*^{(j)}, v_*^{(j)})$ with error, and denote

$$\tilde{\mathbf{a}}_j = \ln\left(\frac{\mathbf{f}_-(x^{(j)}, v^{(j)})}{\tilde{\phi}_{R,1}(x_*^{(j)}, v_*^{(j)})}\right) \tag{56}$$

as the corresponding data at the grid points. By assumption $|\phi_{R,1}(x_*^{(j)}, v_*^{(j)}) - \tilde{\phi}_{R,1}(x_*^{(j)}, v_*^{(j)})| < \varepsilon_m$, one clearly has

$$\mathbf{a}_j - \tilde{\mathbf{a}}_j = \ln\left(\frac{\mathbf{f}_-(x^{(j)}, v^{(j)})}{\phi_{R,1}(x_*^{(j)}, v_*^{(j)})}\right) - \ln\left(\frac{\mathbf{f}_-(x^{(j)}, v^{(j)})}{\tilde{\phi}_{R,1}(x_*^{(j)}, v_*^{(j)})}\right) = \mathcal{O}(\varepsilon_m) \tag{57}$$

if ε_m is small enough to guarantee that $\tilde{\phi}_{R,1}(x_*^{(j)}, v_*^{(j)})$ is away from zero. Thus, by Lemma 5 one obtains

$$a(x_*^{(j)}, v_*^{(j)}) - \tilde{\mathbf{a}}_j = \mathcal{O}(\varepsilon_1^{-2-\delta}\varepsilon^4 + \varepsilon_m)\,.$$

Then replacing $\mathbf{a}$ with $\tilde{\mathbf{a}}$ in the proof of Theorem 4 gives the error estimate (55) under the choice (54). ∎

5. Discussion in diffusive regime. As demonstrated in previous sections, in most optimization formulations of the inverse problem, one always needs a repeated use of the forward solver. However, the RTE resides in a high dimensional phase space, which requires a large amount of computational effort. A well-accepted approximation is the diffusion approximation, which gives rise to a model that only varies in spatial domain. This approximation turns out to be very efficient in the forward setting, but it brings about a huge error in the inverse problem. Studies have shown that, in the case when such an approximation can be made, the recovery of the scattering and absorption coefficient becomes unstable and inaccurate. This phenomena was systematically studied in [13] for the stationary case and in [12] for the time-dependent case, where the Knudsen number (Kn) denotes the regime of the equation: a smaller Knudsen number means better approximation of the diffusion limit. Then it is shown that, as the Knudsen number shrinks to zero, in the forward setting, the RTE converges to the diffusion equation, with its scattering and absorption coefficients becoming the diffusion and the damping coefficients in the diffusion equation, respectively. For the inverse setting, however, the recovery becomes very bad, with the so-defined indistinguishability coefficient—a quantity that measures the accuracy of the recovery—blowing up to infinity in the diffusion regime.

In this section, we will revisit this result in our numerical optimization framework and show that, in a 3D diffusive regime, E_1 cannot be separated from E_2 and E_3, making the algorithm invalid in the very first step. More precisely, the original equation (1) in the diffusive scaling is rewritten as

$$v \cdot \nabla_x f + \left(\mathsf{Kn}\sigma_a(x) + \frac{1}{\mathsf{Kn}}\sigma_\nu(x, v)\right) f = \frac{1}{\mathsf{Kn}} \int k(x, v, v') f(x, v') \mathrm{d}v'\,, \tag{58}$$

where the Knudsen number Kn represents the ratio of the mean free path and the domain length and is an indicator of the regime the equation is in. Here we decompose the total absorption σ in (1) into two components, σ_a and σ_ν. The former is a pure absorption, and the latter is the absorption caused by scattering, i.e., $\sigma_\nu(x, v) = \int k(x, v, v')dv'$. As written in (58), σ_a and σ_ν are rescaled differently. In this new form, the inverse problem will recover either (σ, k) or (σ_a, k).

For simplicity, we consider the domain $\Omega = \left\{x = (x_1, x_2, x_3) \in \mathbb{R}^3, 0 \le x_1 \le 1\right\}$, and thus $\partial\Omega$ are two infinite size parallel walls located at $x_l = (0, 0, 0)$ and $x_r = (1, 0, 0)$, respectively. The outer normal directions are then $n_l = (1, 0, 0)$ and $n_r = (-1, 0, 0)$. The main theorem is stated as follows.

THEOREM 5. *In three dimensions, consider the incoming data given by* $f_-(x', v') = \psi(\frac{|x'-x_0|}{\varepsilon})\psi(\frac{|v'-v_0|}{\varepsilon})$, *with* $x_0 = (0, x_2, x_3)$, *and* E_i *defined as in* (40). *Assuming that* $\partial\Omega$ *is* C^1 *in the neighborhood of* $x_* = x_0 + \tau_+(x_0, v_0)v_0$, *one has*

$$E_1 \le C_1\varepsilon^4 \exp\left(-C_2/\mathsf{Kn}\right), \quad E_3 \ge c\varepsilon^4\varepsilon_1^4\mathsf{Kn}^q\,, \tag{59}$$

where C_1, C_2, c, *and* q *are positive constants, and* q *depends on the dimension of the problem. Consequently, if*

$$\mathsf{Kn} \le \mathcal{O}\left(-\frac{1}{\ln \varepsilon_1}\right),$$

then the algorithm breaks down since E_3 *can no longer be distinguished from* E_1.

The proof of this theorem relies on asymptotic and boundary layer analysis. For this reason, we first consider a 3D case with slab geometry, which essentially reduces to a problem in one dimension. Indeed, denote $x = (x_1, x_2, x_3)$, and then in slab geometry the dependent functions are assumed to be homogeneous in x_2 and x_3, and the velocity is $v = (\cos\theta, 0, 0)$, where θ is the angle between the direction of the flight and positive x_1 direction. Therefore, the photon dynamics varies only along x_1 and v_1, and the problem (58) reduces to the 1D problem

$$\begin{cases} v_1\partial_{x_1} f = \frac{1}{\mathsf{Kn}}\left(\langle f\rangle - f\right), \quad (x_1, v_1) \in [0,1]\times[-1,1]\,, \\ f|_{x_1=0, v_1>0} = \phi(v_1)\,, \\ f|_{x_1=1, v_1<0} = 0\,. \end{cases} \tag{60}$$

Here we assume that the boundary is placed at $x_1 = 0$ and $x_1 = 1$. At the left boundary $x_1 = 1$, there are incoming data $\phi(v_1)$, which could be designed as a concentrated source term. We also assume that $\sigma_a \equiv 0$ just for the ease of computation that follows.

When $\mathsf{Kn} = 1$, equation (60) is a reduced version of RTE (1) in one dimension with $\sigma = k = 1$. Also as $\mathsf{Kn} \to 0$, physically it means the interactions between particles become intense, driving the equation to the diffusive regime. More specifically, we have the next proposition (here we omitted the subscript "1").

PROPOSITION 2. *In the* $\mathsf{Kn} \to 0$ *limit, the solution to* (60) *can be well approximated by*

$$f(x,v) = f^A + E^A = f^L\left(\frac{x}{\mathsf{Kn}}, v\right) + f^I(x,v) + E^A(x,v)\,, \tag{61}$$

where f^A *is the approximate solution and has two parts: the layer part, denoted by* f^L, *and the interior part, denoted by* f^I. E^A *is the approximation error. There exists a constant* η, *such that the layer, the interior, and the error satisfy the following equations, respectively:*

f^L: *The layer lives only within* Kn *distance from* $x = 1$, *and with change of variables* $y = \frac{x}{\mathsf{Kn}}$, *it satisfies*

$$\begin{cases} v\partial_y f^L = \langle f^L\rangle - f^L\,, \\ f^L(y=0, v>0) = \phi(v) - \eta\,, \\ f^L(y=\infty) = 0\,. \end{cases} \tag{62}$$

f^I: *The interior is defined as*

$$f^I(x,v) = \theta - \mathsf{Kn} v \partial_x \theta\,,$$

and with θ *satisfies*

$$\begin{cases} \partial_x^2 \theta = 0\,, \\ \theta(x=0) = \eta\,, \quad \theta(x=1) = 0\,. \end{cases} \tag{63}$$

It also means that f^I *satisfies*

$$\begin{cases} v\partial_x f^I = \frac{1}{\mathsf{Kn}} \left(\langle f^I \rangle - f^I \right)\,, \\ f^I(x=0, v>0) = \eta - \mathsf{Kn} v \partial_x \theta\,, \\ f^I(x=1, v<0) = 0\,. \end{cases} \tag{64}$$

E^A: *The error term satisfies*

$$\begin{cases} v\partial_x E^A = \frac{1}{\mathsf{Kn}} \left(\langle E^A \rangle - E^A \right), \\ E^A(x=0, v>0) = \mathsf{Kn} v \partial_x \theta, \\ E^A(x=1, v<0) = -f^L(\frac{1}{\mathsf{Kn}}, v). \end{cases} \tag{65}$$

Moreover, in a neighborhood of the right wall, with $x \in (1-2\mathsf{Kn}, 1)$,

$$f^I(x) = 1 - x\,, \quad f^L(x) \sim e^{-x/\mathsf{Kn}}\,, \quad E^A \sim e^{-x/\mathsf{Kn}}\,. \tag{66}$$

Proof. To show (61), one simply needs to add up the three equations (62), (64), and (65). The properties in (66) are from the solution to the diffusion equation and the behavior of the layer equation [22]. η is termed the extrapolation length, and its existence is proved in [22], but it cannot be computed explicitly. ∎

Remark 3. In a more general 3D case, the analysis can be a bit complicated. As mentioned earlier in this section, we still assume that the boundaries are two infinite size parallel walls located at $x_l = (0,0,0)$ and $x_l = (1,0,0)$, respectively. Then the equation reads

$$\begin{cases} v_1 \partial_{x_1} f + v_2 \partial_{x_2} f + v_3 \partial_{x_3} f = \frac{1}{\mathsf{Kn}} \mathcal{L}[f]\,, \quad (x_1, x_2, x_3) \in [0,1] \times \mathbb{R}^2\,, \quad \sum_{i=1}^3 v_i^2 = 1\,, \\ f|_{x_1=0, v_1>0} = \phi^x(x_2, x_3) \phi^v(v)\,, \\ f|_{x_1=1, v_1<0} = 0\,. \end{cases}$$

Here $\mathcal{L}[f] = \langle f \rangle - f$ is an abbreviation of the collision term, and ϕ^x and ϕ^v are two functions concentrated at $x_0 = (0,0,0)$ and $v_0 = (1,0,0)$. Namely, the particles getting into the domain are mainly from the origin with speed pointing directly to the wall on the right. As Kn goes to zero, the layer appears only on the left side along the x_1 direction, and by setting

$$y = \frac{x_1}{\mathsf{Kn}}\,,$$

we separate the layer equation and the interior equation as follows:

- Layer:

$$\begin{cases} v_1 \partial_y f^L = \mathcal{L}[f^L]\,, \quad y \in [0, \infty)\,, \\ f^L|_{y=0, v_1>0} = \phi^x(x_2, x_3) \left(\phi^v(v) - \eta \right)\,, \\ f^L|_{y=\infty} = 0\,. \end{cases} \tag{67}$$

- Interior:
(68)
$$\begin{cases} v_1\partial_{x_1}f^I + v_2\partial_{x_2}f^I + v_3\partial_{x_3}f^I = \frac{1}{\mathsf{Kn}}\mathcal{L}[f^I]\,, \quad (x_1,x_2,x_3)\in[0,1]\times\mathbb{R}^2\,,\\ f^I|_{x_1=0,v_1>0} = \eta\phi^x(x_2,x_3)\,,\\ f|_{x_1=1,v_1<0} = 0\,. \end{cases}$$

- Error: the error is defined by
$$E^A = f - f^A = f - f^L - f^I\,,$$
and taking (67) and (68) into account, one gets
(69)
$$\begin{cases} (v_1\partial_{x_1} + v_2\partial_{x_2} + v_3\partial_{x_3})\,E^A = \frac{1}{\mathsf{Kn}}\mathcal{L}[E^A] - (v_2\partial_{x_2} + v_3\partial_{x_3})f^L,\\ \qquad (x_1,x_2,x_3)\in[0,1]\times\mathbb{R}^2\,,\\ E^A|_{x_1=0,v_1>0} = 0\,,\\ E^A|_{x_1=1,v_1<0} = -f^L(\frac{1}{\mathsf{Kn}},x_2,x_3,v)\,. \end{cases}$$

It has been shown in [22] that $f^L(y,v)\in L^2\left(e^{\beta y}\mathrm{d}y, L^2(\mathrm{d}x)\right)$; then in the neighborhood of $x_{0*}=(1,0,0)$, $v_{0*}=(1,0,0)$,
$$f^L(x,v)\sim e^{-\frac{x_1}{\mathsf{Kn}}}\,,\quad E^A(x,v)\sim e^{-\frac{x_1}{\mathsf{Kn}}}\,,$$
and thus $f\sim f^I$ around $x_1=1$. The standard asymptotic analysis applied on f^I shows that
$$f^I = \theta - \mathsf{Kn}v\cdot\nabla_x\theta + \mathsf{Kn}^2(v\cdot\nabla_x)^2\theta + \cdots\,,\qquad \int f^I\mathrm{d}v = \theta\,,$$
where
$$\Delta_x\theta = 0\,,\quad \theta|_{x_1=0} = \eta\phi^x(x_2,x_3)\,,\quad \theta|_{x_1=1} = 0\,,\qquad x_* = (1,0,0)\,.$$
In summary, around x_{0*}, asymptotically we have
$$\int f\mathrm{d}v \sim \int f^I\mathrm{d}v = \theta \sim |x-x_{0*}|^q,$$
with q depending on the dimension ($q=1$ in one dimension, for example).

We would like to point out that the choice of x_0 and v_0 is arbitrary as long as they reside on the left wall. Here we pick $x_0=(0,0,0)$ and $v_0=(1,0,0)$ just as an example. In the following proof of Theorem 5, we still make this choice, and again it can be easily adapted to other choices.

Proof of Theorem 5. It follows from (45) that
$$E_1 \le e^{-C_2/\mathsf{Kn}}\int_{|x'-x_0|<\varepsilon,|v'-v_0|<\varepsilon}\mathrm{d}\xi(x',v')\,,$$
where $C_2=\min_{x',v'}\tau_-((x'+\tau_+(x',v')v'),v')>0$, the minimum taken over all possible (x',v') for which the integrand in (45) is nonzero. Then the upper bound for E_1 (59) follows.

In order to estimate E_3, first notice that for the input $\psi(\frac{|x'-x_0|}{\varepsilon})\psi(\frac{|v'-v_0|}{\varepsilon})$ with $x_0=(0,0,0)$ and $v_0=(1,0,0)$, the asymptotic analysis gives

$$f(x,v)=\theta(x)+\mathcal{O}(e^{-1/\mathsf{Kn}}),\quad \theta(x)\geq c|x-x_*|^q,$$

for some $c>0$, where $x_{0*}=(1,0,0)$. This means that at the receiver placed at x_{0*}, $\theta(x)$ has a polynomial lower bound. Then, for x with $|x-x_{0*}|\leq \mathsf{Kn}$, by using (43), we estimate

$$\begin{aligned}(\mathcal{B}\mathcal{A}^{-1}\mathcal{B}f)(x,v)&=\int_\Omega\int_V K_1(x,v,y,w)f(y,w)\mathrm{d}w\mathrm{d}y\\&=\mathsf{Kn}^{-2}\int_{\Omega_x}e^{-|x-y|/\mathsf{Kn}}\frac{\theta(y)}{|x-y|^2}\mathrm{d}y\\&\geq c\mathsf{Kn}^{-2}\int_{\Omega_x\bigcap\{|x-y|\leq\mathsf{Kn}\}}\frac{|y-x_*|^q}{|x-y|^2}\mathrm{d}y\\&\geq c\mathsf{Kn}^{-2}\int_{\Omega_x\bigcap\{|x-y|\leq|x-x_*|/2\}}\frac{|y-x_*|^q}{|x-y|^2}\mathrm{d}y\,.\end{aligned}$$

Note that if $|x-y|\leq|x-x_*|/2$, then $|y-x_*|\geq|x-x_*|/2$. Thus,

$$(\mathcal{B}\mathcal{A}^{-1}\mathcal{B}f)(x,v)\geq c\mathsf{Kn}^{-2}|x-x_*|^q\int_{\Omega_x\bigcap\{|x-y|\leq|x-x_*|/2\}}\frac{1}{|x-y|^2}\mathrm{d}y\geq c\mathsf{Kn}^{-2}|x-x_*|^{q+1}\,.$$

Since α_3 relates to $\mathcal{A}^{-1}\left(\mathcal{B}\mathcal{A}^{-1}\mathcal{B}\right)$, and by using the assumption that $\partial\Omega$ is C^1 at x_{0*}, we have

$$\begin{aligned}\alpha_3(x_*,v;x',v')&=\int_0^{\tau_-(x_*,v)}e^{-\frac{1}{\mathsf{Kn}}\int_0^t\sigma_\nu(x_*-sv,v)\mathrm{d}s}(\mathcal{B}\mathcal{A}^{-1}\mathcal{B}f)(x_*-tv,v)\mathrm{d}t\\&\geq c\mathsf{Kn}^{-2}\int_0^{\mathsf{Kn}}|(x_*-tv)-x_*|^{q+1}\mathrm{d}t=c\mathsf{Kn}^q\,.\end{aligned}$$

Then the lower bound of E_3 follows directly from its definition in (40). Comparing E_3 and E_1, we see that as long as $\mathsf{Kn}\leq\mathcal{O}(-\frac{1}{\ln\varepsilon_1})$, E_3 is no longer much smaller than E_1, and the separation cannot be done. ∎

6. Numerical results. We demonstrate numerical evidence in this section. More specifically, we will numerically show the results in Theorem 3: as ε becomes small, the input becomes more like a δ-function, and the light propagates more like a beam. When this happens, E_1, the light intensity provided by the ballistic part, becomes dominant, and E_2+E_3, which contains the intensity of scattered photons, diminishes.

For the numerical experiment, we use the following simplified equation (with Kn being the Knudsen number):

$$v\cdot\nabla_x f+\left(\mathsf{Kn}\sigma_a(x)+\frac{1}{\mathsf{Kn}}\right)f=\frac{1}{2\pi\mathsf{Kn}}\int f\mathrm{d}v\quad\text{on}\quad(x,\theta)\in[0,1]^2\times[-\pi,\pi]\,,\tag{70}$$

where $v=(\cos\theta\,,\sin\theta)$ and we have set $\sigma_\nu=k=1$, and the absorption coefficient is

$$\sigma_a(x,y)=1+0.1\chi_{(x-0.5)^2+(y-0.5)^2\leq0.09},$$

where χ is a characteristic function.

For this specific geometry, the inflow boundary consists of the four parts

$$\Gamma_- = \{x = 0, \cos\theta > 0\} \cup \{x = 1, \cos\theta < 0\} \cup \{y = 0, \sin\theta > 0\} \cup \{y = 1, \sin\theta < 0\},$$

and the incoming data are given by

$$f_{\Gamma_-} = \psi\left(\frac{|x - x_0|}{\varepsilon}\right)\psi\left(\frac{|v - v_0|}{\varepsilon}\right).$$

They converge to a δ-function as ε shrinks.

For discretization, we sample $(N_x+1)^2$ in the spatial domain, located at $(i\Delta x, j\Delta x)$, $i, j = 0, \ldots, N_x$, with $\Delta x = 1/N_x$, and N_θ grid points in θ, located at $-\pi+(i+1/2)\Delta\theta$, with $\Delta\theta = 2\pi/N_\theta$. A GMRES-type algorithm is used [23]. Numerically the boundary condition is set as

$$f|_{\Gamma_-} = \begin{cases} c_\varepsilon & \text{if } x = 0,\ |y - 1/2| \le \varepsilon,\ |\theta| \le \pi\varepsilon, \\ 0 & \text{otherwise.} \end{cases}$$

Here $c_\epsilon > 0$ is a normalizing constant such that the local intensity $\rho(x, y) = \int f(x, y, \theta)\mathrm{d}\theta$ of the solution to (58) has maximum 1. For accuracy, we set $N_x = N_\theta = 160$, and the computation is done with $\varepsilon = 2^{-3}, 2^{-4}, 2^{-5}, 2^{-6}$ for Kn being 1, 2^{-1}, and 2^{-2}. We have to emphasize that the geometry and the inflow condition in this example are simple enough for the direct GMRES to be applied, but typically the beam inserted at $(x_j, v_j) \in \Gamma_-$ may not have its counterpart on the discretized Γ_+, and more sophisticated sampling strategies are called for, as shown in [25].

The goal is to show that as ε shrinks, E_1 becomes dominant. Since E_1 presents the intensity contained in the ballistic part, we can consider it as the integration at the boundary of f, the solution to the following equation:

$$v \cdot \nabla_x f + \left(\mathsf{Kn}\sigma_a(x) + \frac{1}{\mathsf{Kn}}\right) f = 0 \quad \text{on} \quad (x, \theta) \in [0, 1]^2 \times [-\pi, \pi]. \tag{71}$$

Then comparing E_1 to $E_1 + E_2 + E_3$ amounts to comparing the solutions to (70) and (71). The two solutions should demonstrate more similarity when ε is small, and in the small Kn regime, the scattering term is magnified and strong, and the two solutions are more distinct.

These are numerically justified in Figures 1 and 2. In particular, in Figure 1 we compare $\int f\mathrm{d}v$ computed from (70) and (71) with different ε for three sets of Kn. For all Kn, as ε shrinks, the two solutions are visually more equivalent, and small Kn gives more distinct solutions.

In Figure 2, we compare the intensity of the outflow at boundary $\{x=1, \cos\theta>0\}$. We plot

$$g(y) = \int_{\cos\theta>0} f(1, y, \theta)\cos\theta\mathrm{d}\theta \tag{72}$$

as a function of y. It is also clear that larger Kn and smaller ε lead to closer intensities between the two solutions.

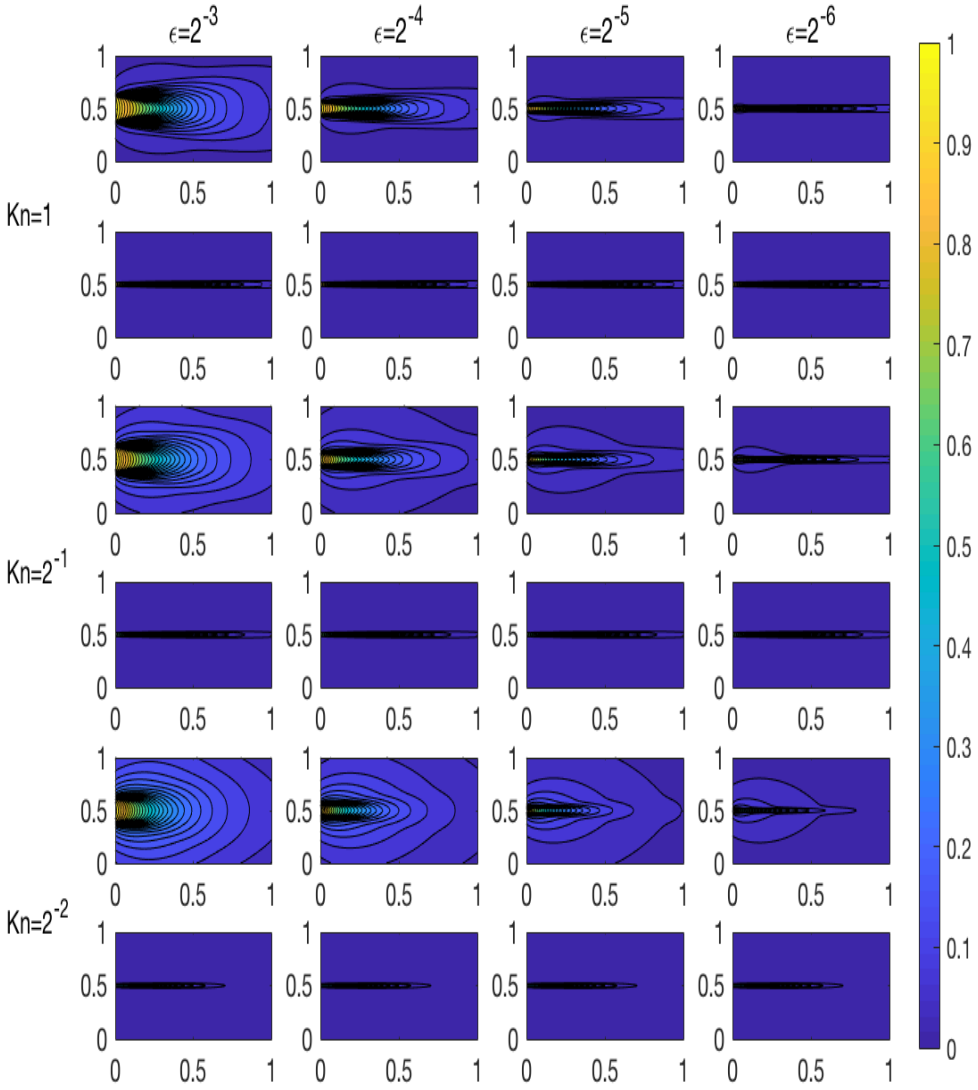

FIG. 1. *For* $\mathsf{Kn} = 1$, 2^{-1}, *and* 2^{-2}, *we compare the solution to the RTE* (70) *and the solution to the equation without the scattering term (X-ray transform), written in* (71), *using different* ε *in the incoming data. For each* Kn, *the top row shows* ρ *computed from* (70), *and the second row shows the solution to* (71), *the X-ray transform solution that contains the ballistic part of the information. It is obvious that for* $\mathsf{Kn} = 1$, *a smaller* ε, *which means finer incoming data, leads to better approximations: the two solutions are more similar. The same trend is observed for* $\mathsf{Kn} = 2^{-1}$ *and* $\mathsf{Kn} = 2^{-2}$. *The difference between the two solutions also depends on the regime that the system is in: a smaller* Kn *leads to stronger scattering, which means the solutions to the RTE and the X-ray transform are increasingly different.*

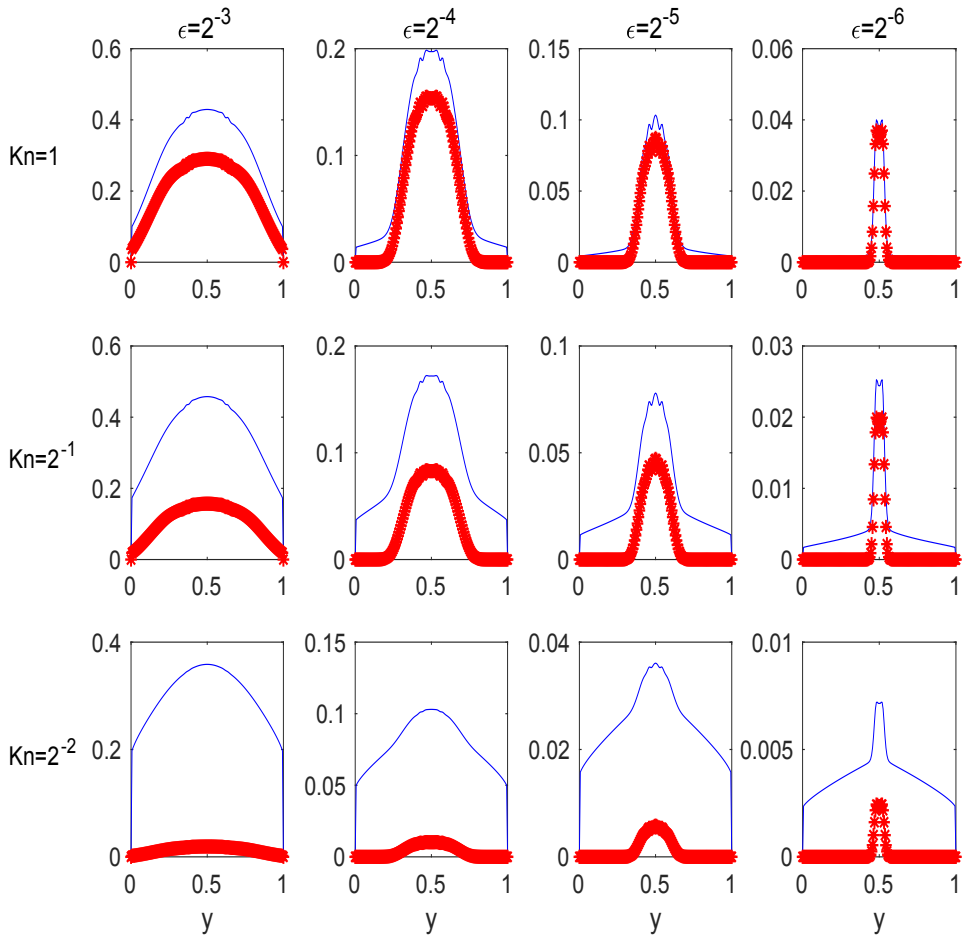

FIG. 2. *Outflow intensity $g(y)$ from* (72)*: in all of the plots, the star line shows the solution to the X-ray transform, the intensity given by the solution to* (71)*, and the solid line shows the solution to the RTE* (70)*, with different sets of* Kn *and ε in the incoming data. As ε becomes small, the ballistic part dominates and the solution to the two equations converges, and as* Kn *becomes small, the scattering effect is strong and the disparities between the two solutions becomes strong.*

REFERENCES

[1] G. Abdoulaev, K. Ren, and A. Hielscher, *Optical tomography as a PDE-constrained optimization problem*, Inverse Problems, 21 (2005), pp. 1507–1530.

[2] S. Arridge, *Optical tomography in medical imaging*, Inverse Problems, 15 (1999), pp. R41–R93.

[3] S. R. Arridge and J. C. Schotland, *Optical tomography: Forward and inverse problems*, Inverse Problems, 25 (2009), 123010.

[4] G. Bal, *Inverse transport theory and applications*, Inverse Problems, 25 (2009), 053001.

[5] G. Bal, F. J. Chung, and J. C. Schotland, *Ultrasound modulated bioluminescence tomography and controllability of the radiative transport equation*, SIAM J. Math. Anal., 48 (2016), pp. 1332–1347, https://doi.org/10.1137/15M1026262.

[6] G. Bal and A. Jollivet, *Time-dependent angularly averaged inverse transport*, Inverse Problems, 25 (2009), 075010.

[7] G. Bal, I. Langmore, and F. Monard, *Inverse transport with isotropic sources and angularly averaged measurement*, Inverse Probl. Imaging, 2 (2008), pp. 23–42.

[8] G. Bal and A. Tamasan, *Inverse source problems in transport equations*, SIAM J. Math. Anal., 39 (2007), pp. 57–76, https://doi.org/10.1137/050647177.

[9] C. Bontus and T. Kohler, *Reconstruction algorithms for computed tomography*, Advances in Imaging and Electron Physics, 151 (2008), pp. 1–63.

[10] A. V. Bronnikov, *Numerical solution of the identification problem for the attenuated radon transform*, Inverse Problems, 15 (1999), pp. 1315–1324.

[11] K. Chen, Q. Li, and J.-G. Liu, *Online learning in optical tomography: A stochastic approach*, Inverse Problems, 29 (2018), 075010.

[12] K. Chen, Q. Li, and L. Wang, *Stability of inverse transport equation in diffusion scaling and Fokker–Planck limit*, SIAM J. Appl. Math., 78 (2018), pp. 2626–2647, https://doi.org/10.1137/17M1157969.

[13] K. Chen, Q. Li, and L. Wang, *Stability of stationary inverse transport equation in diffusion scaling*, Inverse Problems, 34 (2018), 025004.

[14] Y. Cheng, I. M. Gamba, and K. Ren, *Recovering doping profiles in semiconductor devices with the Boltzmann-Poisson model*, J. Comput. Phys., 230 (2011), pp. 3391–3412.

[15] M. Choulli and P. Stefanov, *An inverse boundary value problem for the stationary transport equation*, Osaka J. Math., 36 (1998), pp. 87–104.

[16] S. Douté, B. Schmitt, R. Lopes-Gautier, R. Carlson, L. Soderblom, J. Shirley, and the Galileo NIMS Team, *Mapping So2 frost on Io by the modeling of NIMS hyperspectral images*, Icarus, 149 (2001), pp. 107–132.

[17] H. W. Engl, M. Hanke, and A. Neubauer, *Regularization of Inverse Problems*, Springer Netherlands, 1996.

[18] A. Katsevich, *Analysis of an exact inversion algorithm for spiral cone-beam CT*, Phys. Med. Biol., 47 (2002), pp. 2583–2597.

[19] A. Katsevich, *An improved exact filtered backprojection algorithm for spiral computed tomography*, Adv. Appl. Math., 32 (2004), pp. 681–697.

[20] A. Katsevich and M. Kapralov, *Filtered backprojection inversion of the cone beam transform for a general class of curves*, SIAM J. Appl. Math., 68 (2007), pp. 334–353, https://doi.org/10.1137/060673187.

[21] O. Lehtikangas, T. Tarvainen, A. Kim, and S. Arridge, *Finite element approximation of the radiative transport equation in a medium with piece-wise constant refractive index*, J. Comput. Phys., 282 (2015), pp. 345–359.

[22] Q. Li, J. Lu, and W. Sun, *A convergent method for linear half-space kinetic equations*, ESAIM M2AN, 51 (2017), pp. 1583–1615.

[23] Q. Li and L. Wang, *Implicit asymptotic preserving method for linear transport equations*, Commun. Comput. Phys., 22 (2017), pp. 157–181.

[24] M. Machida and J. C. Schotland, *Inverse Born series for the radiative transport equation*, Inverse Problems, 31 (2015), 095009.

[25] F. Monard and G. Bal, *An accurate solver for forward and inverse transport*, J. Comput. Phys., 229 (2010), pp. 4952–4979.

[26] L. D. Montejo, J. Jia, H. K. Kim, U. J. Netz, S. Blaschke, G. A. Müller, and A. H. Hielscher, *Computer-aided diagnosis of rheumatoid arthritis with optical tomography, part* 1: *Feature extraction*, J. Biomed. Opt., 18 (2013), 076001.

[27] L. D. Montejo, J. Jia, H. K. Kim, U. J. Netz, S. Blaschke, G. A. Müller, and A. H. Hielscher, *Computer-aided diagnosis of rheumatoid arthritis with optical tomography, part* 2: *Image classification*, J. Biomed. Opt., 18 (2013), 076002.

[28] F. Natterer, *The Mathematics of Computerized Tomography*, Classics Appl. Math. 32, SIAM, Philadelphia, 2001, https://doi.org/10.1137/1.9780898719284.
[29] K. Ren, *Recent developments in numerical techniques for transport-based medical imaging methods*, Commun. Comput. Phys., 8 (2010), pp. 1–50.
[30] K. Ren, R. Zhang, and Y. Zhong, *Inverse transport problems in quantitative PAT for molecular imaging*, Inverse Problems, 31 (2015), 125012.
[31] T. Saratoon, T. Tarvainen, B. T. Cox, and S. R. Arridge, *A gradient-based method for quantitative photoacoustic tomography using the radiative transfer equation*, Inverse Problems, 29 (2013), 075006.
[32] T. Tarvainen, B. T. Cox, J. P. Kaipio, and S. R. Arridge, *Reconstructing absorption and scattering distributions in quantitative photoacoustic tomography*, Inverse Problems, 28 (2012), 084009.
[33] T. Tarvainen, V. Kolehmainen, S. R. Arridge, and J. P. Kaipio, *Image reconstruction in diffuse optical tomography using the coupled radiative transport–diffusion model*, J. Quant. Spectroscopy Radiative Transfer, 112 (2011), pp. 2600–2608.
[34] T. Tarvainen, V. Kolehmainen, A. Pulkkinen, M. Vauhkonen, M. Schweiger, S. R. Arridge, and J. P. Kaipio, *An approximation error approach for compensating for modelling errors between the radiative transfer equation and the diffusion approximation in diffuse optical tomography*, Inverse Problems, 26 (2010), 015005.
[35] C. R. Vogel, *Computational Methods for Inverse Problems*, Frontiers Appl. Math. 23, SIAM, Philadelphia, 2002, https://doi.org/10.1137/1.9780898717570.